



La doped AlPO-5: Enhanced NH₃ sensing properties, thermodynamic investigation and humidity-enhanced effect



Luyu Wang^{a,*}, Yunling Wu^b, Junkuo Gao^{a,**}, Jia Song^{c,***}

^a Institute of Fiber Based New Energy Materials, The Key Laboratory of Advanced Textile Materials and Manufacturing Technology of Ministry of Education, College of Materials and Textiles, Zhejiang Sci-Tech University, Hangzhou, 310018, PR China

^b Jiangsu Key Laboratory for Carbon-Based Functional Materials & Devices, Institute of Functional Nano and Soft Materials (FUNSOM), Soochow University, Suzhou, 215123, PR China

^c Shanghai Engineering Research Center of 3D Printing Materials, Shanghai, 200437, PR China

ARTICLE INFO

Keywords:

AlPO-5
La doping
Gas sensors
Ammonia
Quartz crystal microbalance (QCM)

ABSTRACT

Solid AlPO-5 and La doped AlPO-5 (La/AlPO-5) were synthesized by a hydrothermal treatment followed by crystallization and calcination. The ammonia (NH₃) sensing properties of AlPO-5 and La/AlPO-5 were evaluated by using quartz crystal microbalance (QCM) platform to work out the enhanced effect of La doping treatment. La/AlPO-5 possessed a higher response to NH₃ than that of AlPO-5 with same concentration. In addition to the favorable sensitivity, La/AlPO-5 based sensor also showed prominent repeatability and selectivity. We also explored the thermodynamics and humidity-enhanced effect in the NH₃ sensing process.

1. Introduction

Ammonia (NH₃) is a common harmful gas comes from chemical plant leakage and fertilizer abuse and leads to mucosal damage, dyspnea, skin burn, etc. [1,2]. However, the use of NH₃ in the fields of fertilizer synthesis and fiber manufacturing is inevitable [3]. As a result, rapid detection of NH₃ gas at very low concentration is essential to its transport, storage and usage. Gas sensors are recognized as ideal devices which are capable of detecting gases. High sensitivity, excellent selectivity and reversibility are crucial desired parameters of sensor quality [4].

Quartz crystal microbalance (QCM), also known as a precise weighing equipment, is an emerging gas sensing transducer constructed from quartz wafer and metallic electrode. Based on Sauerbrey equation, the change of surface quality of QCM can be transformed into signal of frequency change [5]. Due to its surface modifiability, various specific sensing materials can detect different hazardous gases based on QCM transducer by adsorption [6]. QCM gas sensors have many advantages, such as high sensitivity at ng level, quantifiability for gas concentration, gas discriminability with e-nose, tunable selectivity, low power consumption, and so on [7]. Besides, QCM sensors are convenient to set up, operate and intelligentize [8]. Based on QCM platform, there are some

materials have been used to detect NH₃, such as zinc oxide, graphene oxide isolation layer, phenylacetic acid-modified nanofibrous polystyrene, graphene/polyaniline nanocomposite and so on [9–23]. However, the detection limits of these NH₃ sensors can only reach ppm concentration level, which is not conducive to the timely prevention of NH₃ leakage. One of the glaring advantages of QCM sensor over other sensors is excellent sensitivity, so it is necessary to explore novel sensing materials that can detect NH₃ in ppb concentration level. In addition, few of these reports on QCM NH₃ sensor explored the permanent impact of environmental humidity on the NH₃ sensing response.

AlPO-5 is a high stable solid zeolite material with porous framework, and has been attracted attention in the field of catalysis [24,25]. An exciting property of AlPO-5 zeolite is that Al and/or P can be replaced by other elements to form doped AlPO-5 zeolites with enhanced applied property [26]. Compared with other zeolites, AlPO-5 possesses excellent water stability and thermal stability, which makes it possible to be used in gas sensors based on adsorption.

Herein, solid La doped AlPO-5 (La/AlPO-5) is first reported as QCM surface sensitizing material to efficiently detect NH₃ with high sensitivity, excellent repeatability, and satisfactory selectivity, as shown in Scheme 1. The sensitivity to NH₃ of La/AlPO-5 was greatly improved than undoped AlPO-5, which should be attributed to the added active

* Corresponding author.

** Corresponding author.

*** Corresponding author.

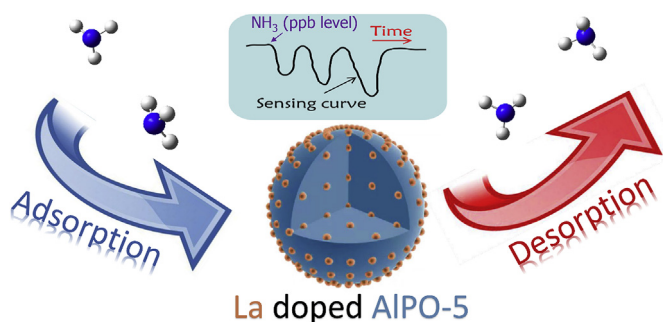
E-mail addresses: wly420219156@163.com (L. Wang), jkgao@zstu.edu.cn (J. Gao), skylve@t.shu.edu.cn (J. Song).

<https://doi.org/10.1016/j.jssc.2019.05.043>

Received 24 March 2019; Received in revised form 14 May 2019; Accepted 24 May 2019

Available online 25 May 2019

0022-4596/© 2019 Elsevier Inc. All rights reserved.



Scheme 1. Based on QCM platform, the La doped AlPO-5 can detect NH₃ gas of ppb concentration.

hydroxyl groups. The detection limit of the La/AlPO-5 can reach 60 ppb. Besides, thermodynamic experiment revealed that the sensing of NH₃ by La/AlPO-5 is attributed to weak physical adsorption. In view of the disadvantage that NH₃ sensing is susceptible to environmental humidity, we explored the enhancement of relative humidity on the response of NH₃ gas. The added response can be corrected by using electronic data compensation in the future.

2. Experimental

2.1. Synthesis of La doped AlPO-5 and AlPO-5

All the reagents were purchased from Aladdin Industrial Corporation. La doped AlPO-5 zeolite was hydrothermally synthesized from an aluminophosphate gel containing Tetramethylguanidine (TMG). As a typical synthesis procedure, aluminum isopropoxide (18.31 g) were added into deionized water (31.6 ml), followed addition of H₃PO₄ (7.2 ml). After formatting gel, of lanthanum (III) nitrate hexahydrate (0.58 g) and TMG (4.4 ml) were introduced. Then, the above mixture was transferred into an autoclave and heated in an oven at 150 °C for 6 h. After the hydrothermal process, the product was collected and dried, then calcined at 550 °C for 5 h. The zeolite product was named as La/AlPO-5. The synthetic procedure of AlPO-5 was the same as the synthesis of La/AlPO-5 except the introduction of lanthanum (III) nitrate hexahydrate.

2.2. Characterization

The morphology of La/AlPO-5 was observed by scanning electron microscope (SEM) (HITACHI S-4800). The Element composition of La/AlPO-5 was collected by X-ray Photo-electron Spectroscopy (XPS) (ESCALAB 250Xi). Wide angle X-ray diffraction patterns of the materials were obtained on a Rigaku DLMAX-2550 diffractometer using Cu KR radiation. Nitrogen adsorption-desorption isotherms were measured at 77 K by using a surface area and porosity analyzer (Micromeritics ASAP 2020). The materials were degassed before the measurements. The BET method was used to extract the specific surface areas. The amounts of various elements in La/AlPO-5 were determined by using inductively coupled plasma atomic emission spectroscopy (ICP-AES) Varian 710-ES. Infrared spectra were analyzed with a Nicolet Avatar-370 FT-IR spectrometer utilizing KBr pellets in the region of 4000–400 cm⁻¹. Thermal analysis was completed on a Mettler Toledo TGA/SDTA85e thermal analyzer, the sample was heated from 30 °C to 800 °C at a rate of 10 °C/min in N₂ atmosphere.

2.3. QCM sensor configuration and experiment setup

The QCM based gas sensing experiments were performed by using a modified setup at 298 K [23]. The water dispersion of zeolites was drop-casted onto the surface of QCM electrode, and the as-fabricated sensor was dried thoroughly. The sensor was tested in a closed

chamber which was placed in a thermostat. Before the measurement, the sensor was exposed to a N₂ stream (15 sccm) until obtained a stable base-line. The analyte was introduced into the chamber with a heater which can evaporate the liquid analyte. Then, the sensor was exposed to the analyte stream until a stable response was obtained. After each response cycle, nitrogen stream would get rid of the analyte to re-establish the baseline.

3. Results and discussion

3.1. Preparation and characterization of La/AlPO-5 and AlPO-5

As shown in Fig. 1a, the XRD pattern indicate that AlPO-5 and La/AlPO-5 all have an AFI structure and well indexed to hexagonal phase AlPO-5 (JCPDS no. 41–0044). But after La doping, the peak of XRD shifts slightly to the left, because its lattice constant is increased because of the doping of La atom which has larger atomic radius than Al atom and P atom. As shown in the insert of Fig. 1a, the amplified XRD pattern clearly shows that the peak of AlPO-5 in the 2θ range of 7°–8° is shifted after doping La. It is indicating that La is well doped into the inherent framework of AlPO-5. In the framework of AlPO-5, AlO₄ tetrahedron and PO₄ tetrahedron are interlinked alternately. The Al or/and P sites on the skeleton can be doped by other doping metal elements, this process is called isomorphism substitution. The isomorphism substitution can be divided into three types: doping into Al sites, doping into P sites, and doping into Al and P sites. The type of substitution mechanism depends on the valence state of the doping element, not the ionic radius. One-valence, divalent, and trivalent metallic elements will replace Al sites. Tetravalent and pentavalent metallic elements will replace P sites. Only silicon (Si) element can replace both Al and P sites [27–29]. It is obvious that trivalent La is doped into Al sites in the framework of AlPO-5. As shown in Fig. 1b, the XPS spectrum of La/AlPO-5 indicates that the material contains Al, P, and O elements which all possess peak. Besides, the peak of La 3d is also shown in Fig. 1b. This peak has a typical La (III) spectrum, indicating that La has occupied some Al (III) sites and doped the framework of AlPO-5. As shown in Fig. 1c, the nitrogen adsorption/desorption isotherms of AlPO-5 and La/AlPO-5 belong to typical H4 hysteresis loop, it should be attributed to their nanoporous topology structures. The specific surface area of AlPO-5 and La/AlPO-5 is 130.72 cm²/g and 107.03 cm²/g, respectively. In the relative pressure range of 0.4–0.6 occurs a slow increase in the adsorption amount, indicating the presence of mesopores. In the relative pressure range of 0.8–1.0, the nitrogen adsorption capacity still increases, indicating the presence of large pores. These conclusions are in accordance with the pore size distribution diagram (the insert of Fig. 1c). The SEM image (Fig. 1d) shows the morphology of La/AlPO-5 is spherical with a diameter of 8–16 μm.

The SEM image of single La/AlPO-5 microsphere together with selected-area element analysis maps of O, Al, P and La in Fig. 2a indicates that all O (cyan), Al (yellow), P (red) and La (green) atoms are distributed uniformly through the whole selected-area, revealing a homogeneous distribution of La in the framework of AlPO-5. This single La/AlPO-5 microsphere was also used for the energy dispersive spectra (EDS) point analyses (see Fig. 2b), demonstrating the coexistence of O, Al, P and La atoms distributed on the surface of La/AlPO-5 microsphere. The overall composition of La/AlPO-5 was obtained from inductively coupled plasma atomic emission spectroscopy (ICP-AES) analysis (shown in Table 1). The amounts of O, Al, P, and La in La/AlPO-5 are 53.15, 20.48, 24.77, and 1.60 wt%, respectively.

Fig. 3a presents the FT-IR spectra of La/AlPO-5 and AlPO-5. The peaks appearing at 1108 cm⁻¹, 717 cm⁻¹ and 467 cm⁻¹ were characteristic of AlPO-5. The peak appearing at 1108 cm⁻¹ is attributed to the asymmetric stretching vibration of the P–O–Al unit. The peak appearing at 717 cm⁻¹ is attributed to the P–O–P or P–O–Al or Al–O–Al symmetrical stretching vibration in the AlPOs material. The peak appearing at 467 cm⁻¹ is attributed to the P–O or Al–O bending vibrations in the AlPOs material.

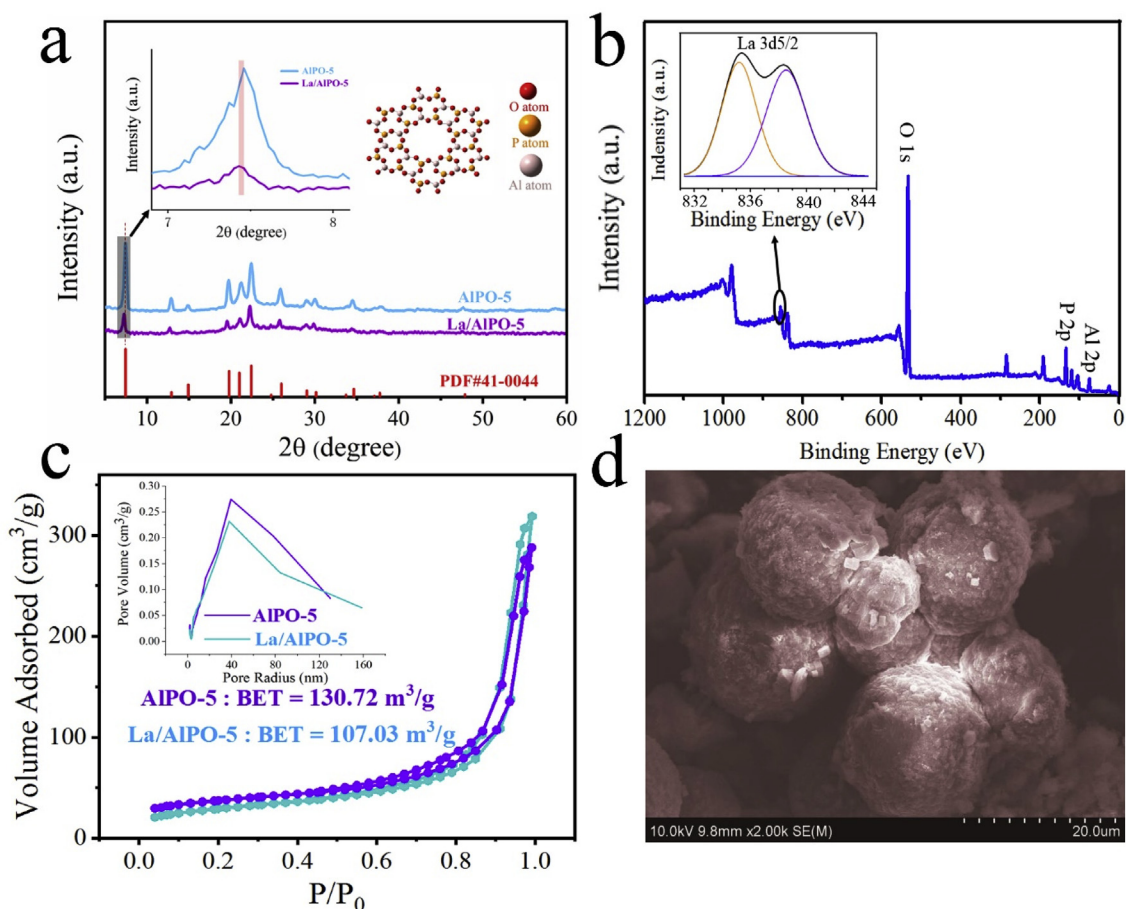


Fig. 1. (a) XRD pattern of La/AlPO-5 and AlPO-5. The insert is the amplified XRD pattern in the 2θ range of 7° – 8° . (b) XPS analyses of La/AlPO-5. (c) N_2 sorption isotherm curves and pore size distribution curves of La/AlPO-5 and AlPO-5. (d) SEM image of La/AlPO-5.

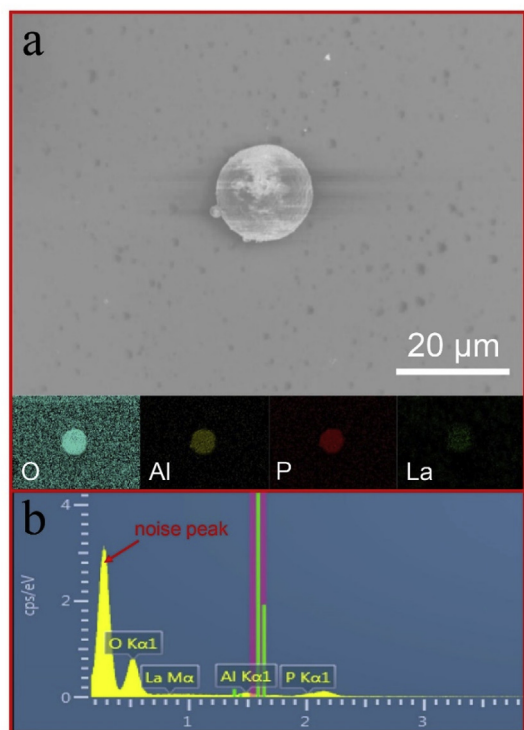


Fig. 2. (a) Elemental mapping characterization of prepared La/AlPO-5. (b) EDS profile obtained from La/AlPO-5.

Table 1

Relative compositions of O, Al, P, and La atoms obtained from ICP-AES analysis.

Element	Amount (wt%)
O	53.15
Al	20.48
P	24.77
La	1.60

These peaks are consistent with the FT-IR data of AlPO-5 in the reported research, indicating the successful synthesis of AlPO-5 [24]. Besides, compared with AlPO-5, the vibration bands of La/AlPO-5 in the region of 1097 cm^{-1} , 715 cm^{-1} and 466 cm^{-1} were shifted to lower wavenumbers. It should be attributed to the longer length of La–O bond than that of Al–O band. These FT-IR data indicating the successful doping of La in the framework of AlPO-5. Fig. 3b shows the thermogravimetric (TG) curves of the calcined La/AlPO-5 and AlPO-5. Most of the weight loss occurs at about 100°C , which is related to the loss of adsorbed water molecules existing in the materials. The total weight loss rate of calcined La/AlPO-5 is about 5% and the total weight loss rate of calcined AlPO-5 is about 3%. It is indicating that La/AlPO-5 can adsorb more water molecules in the air than AlPO-5. This TG test indicating that both La/AlPO-5 and AlPO-5 materials are stable at temperatures as high as 800°C .

3.2. Gas-sensing properties

We first studied the selectivity of La/AlPO-5 and AlPO-5 via using seven kinds of interfering gases at a concentration of 100 ppm (Fig. 4a). It

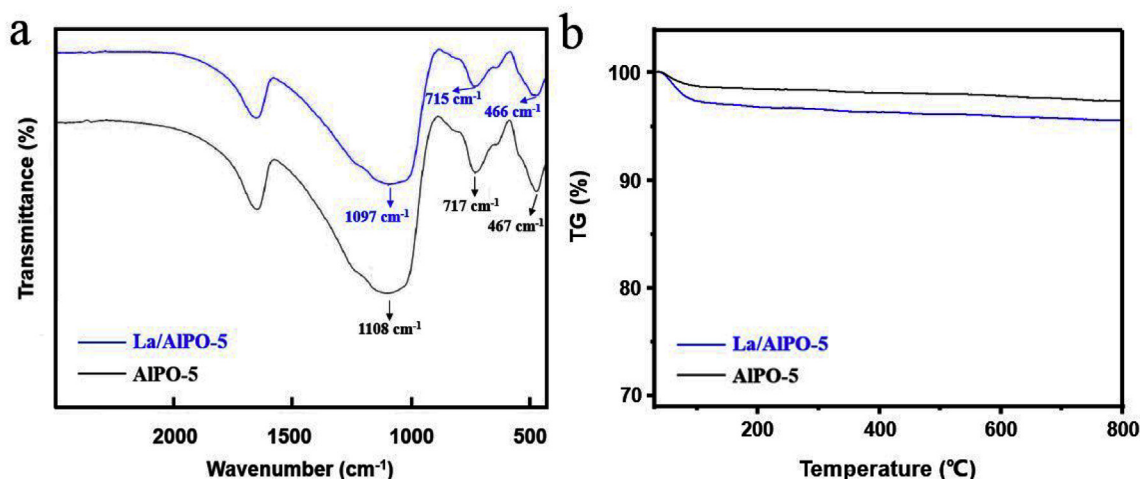


Fig. 3. (a) FT-IR spectra of La/AlPO-5 and AlPO-5. (b) TG curves of La/AlPO-5 and AlPO-5.

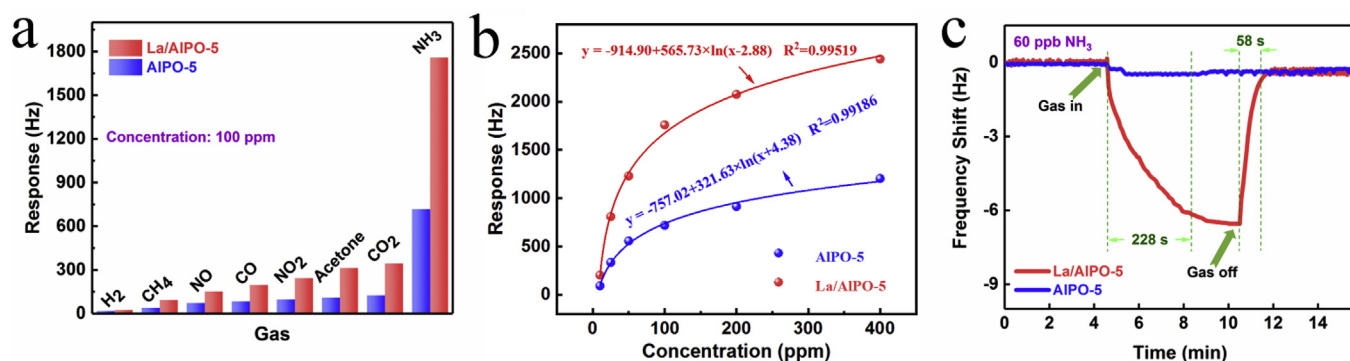


Fig. 4. (a) Selectivity of La/AlPO-5 and AlPO-5. (b) The relationship between the response signals of materials and the NH_3 concentrations (c) Typical response signals of La/AlPO-5 and AlPO-5 to 60 ppb NH_3 .

is indicating that La/AlPO-5 shows a highest response value to NH_3 than other gases, and the response value of La/AlPO-5 to NH_3 is approximately 2.5 times higher than that of AlPO-5. The sensors based on AlPO-5 and La/AlPO-5 samples were tested in NH_3 with different concentrations to evaluate NH_3 sensing characteristics. Fig. 4b plots the relationship between NH_3 concentration (x) and response (y) for the sensors based on AlPO-5 and La doped AlPO-5 (La/AlPO-5). The corresponding equations are $y = -757.02 + 321.63 \times \ln(x+4.38)$ and $y = -914.90 + 565.73 \times \ln(x-2.88)$, respectively, and the regression coefficients (R^2) are 0.99186 and 0.99519 for AlPO-5 and La/AlPO-5, respectively. It is indicating that these two materials exhibited logarithm relationship between the NH_3 concentration and response. Besides, the response of La/AlPO-5 based sensor exhibits a higher response and to NH_3 gas than that of AlPO-5 in the whole concentration range (10 ppm–400 ppm). Fig. 4c shows the response curves of the two materials to 60 ppb NH_3 . It is indicating that the response of La/AlPO-5 is more than 6 Hz, and the response time and recovery time is 228 s and 58 s, respectively. On the contrary, the response of AlPO-5 is negligible. These experimental results suggesting better selectivity and sensitivity of La/AlPO-5. Table 2 lists the detection limits of some NH_3 sensing materials (including La doped AlPO-5 of this paper) based on the QCM platform. The detection limits of these reported NH_3 sensing materials can only reach ppm concentration level, but La doped AlPO-5 can detect NH_3 gas of 60 ppb concentration, indicating its advantage of detecting low concentration NH_3 .

The characterization part of results mentioned that the specific surface area of AlPO-5 is larger than that of La/AlPO-5, so the increased response and enhanced sensitivity of La/AlPO-5 compared with AlPO-5 to NH_3 might be ascribed to the following aspects: (i) When La is

Table 2

Comparison between QCM based NH_3 sensors in reported work and this work.

Reference	Material	Detection limit
[9]	zinc oxide	50 ppm
[10]	graphene oxide	100 ppm
[11]	phenylacetic acid-modified nanofibrous polystyrene	1.5 ppm
[12]	graphene/polyaniline	10 ppm
[13]	clay/polyelectrolyte	1 ppm
[14]	Pd ²⁺ doped ZnO	30 ppm
[15]	Plasma-Polymerized Membrane	500 ppm
[16]	Cellulose acetate nanofibers coated with polyethylenimine and graphene oxide	1 ppm
[17]	Graphene oxide/polystyrene	1 ppm
[18]	dirhodium(II,II) complex	1 wt%
[19]	poly (styrene- <i>block</i> -maleic acid)	1.5 ppm
[20]	carbon nanotubes	6.7 ppm
[21]	silica nanoparticles/poly(allylamine hydrochloride)	2 ppm
[22]	Zn-Porphyrin Networks	10 ppm
[23]	aldehyde-functionalized mesoporous SBA-15	1 ppm
This paper	La doped AlPO-5	Less than 60 ppb

added into the AlPO-5 framework, the zeolite will possess structural defects. The doped La can provide extra hydroxyl sites on its surface, which can adsorb NH_3 by N–H ... O weak hydrogen bond [30]. Besides, when the ratio of aluminum and phosphorus changes, in order to maintain the neutrality of zeolites, P–OH or Al–OH will be produced, these functional groups also enhance the ability to adsorb NH_3 [31]. (ii) The ability of zeolite to adsorb external gas molecule by hydrogen bond adsorption is related to the difference of electronegativity between Al

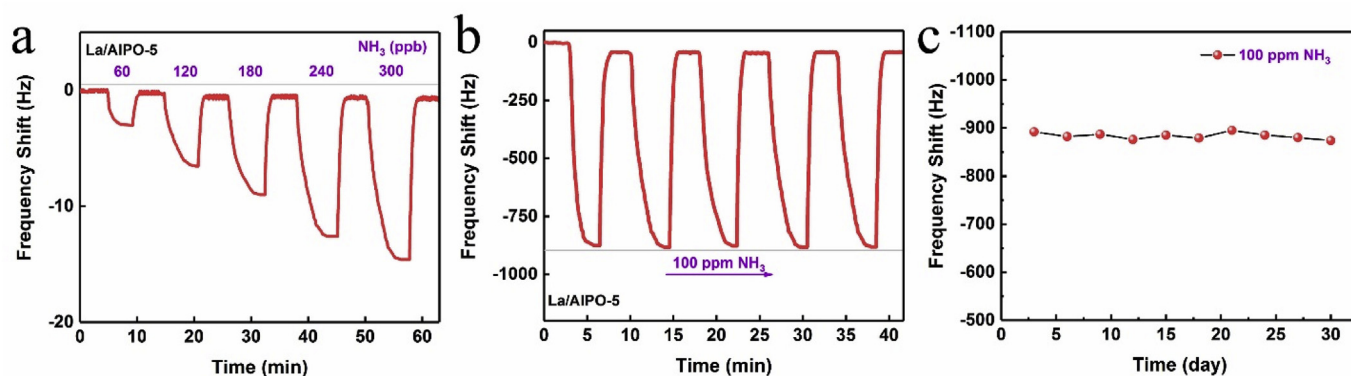


Fig. 5. (a) Real-time dynamic response curve of La/AlPO-5 exposure to NH₃ with increasing concentration. (b) Repeatabile and reversible sensing response of La/AlPO-5 to 100 ppm NH₃. (c) Frequency shifts of La/AlPO-5 to 100 ppm NH₃ as a function of time.

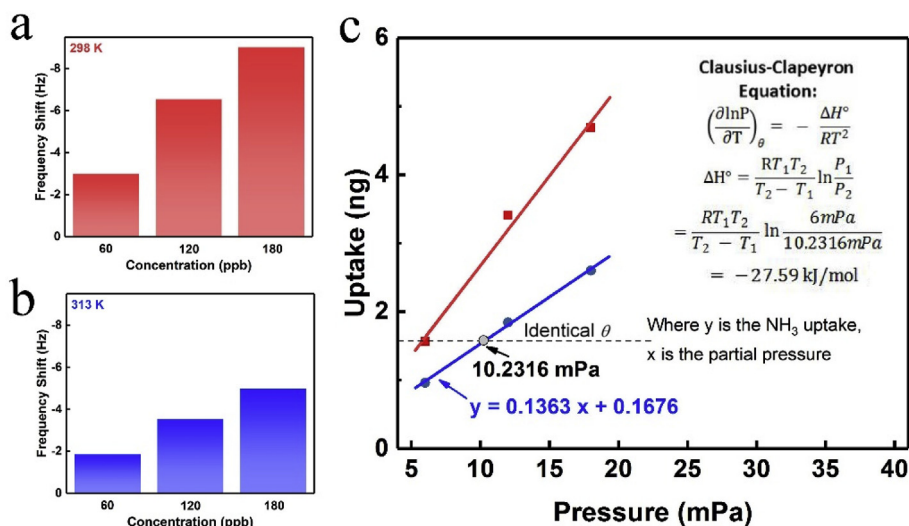


Fig. 6. Gravimetric curves of La/AlPO-5 at 298 K (a) and 313 K (b) to NH₃ with different concentrations of 60, 120, and 180 ppb, respectively. On the basis of the temperature-varied micro-gravimetric curves, the plotted isotherms are used to extract the thermodynamic parameter of adsorption enthalpy (ΔH). (c) Based on the experimental results in (a) and (b), two isotherms are plotted to calculate the value of ΔH .

(1.6) and P (2.2) [32]. The doping of La (electronegativity 1.1) enhances the difference of electronegativity between metal atom and P atom. Thus, the adsorption capacity of AlPO-5 is enhanced. In brief, addition of trace La in AlPO-5 zeolite can improve its NH₃ absorption capacity.

We further studied the sensing performance of La/AlPO-5 to NH₃. Fig. 5a shows the continuous real-time response curve of the La/AlPO-5 to low concentrations of NH₃ range from 60 ppb to 400 ppb. The response to each test is excellent and can be recovered quickly. It is indicating that La/AlPO-5 based sensor can work stably at the concentration of ppb level. The five consecutive responses of La/AlPO-5 to the 100 ppm NH₃ are shown in Fig. 5b, indicating the continuous detection ability in a short period of time. Furthermore, as shown in Fig. 5c, the response of the La/AlPO-5 to 100 ppm NH₃ is also less fluctuating within 30 days, indicating that the sensor can detect NH₃ stably for a long time.

The working basis of mass-sensitive platform, including QCM platform, is the adsorption between sensing material and gas. Based on verified thermodynamic experiment, we can extract the adsorption enthalpy (ΔH) and determine the adsorption mode of the sensing material to the target gas [33–36]. We measured the response of La/AlPO-5 to several low-concentration NH₃ at 298 K and 313 K, respectively, and converted the response to the value of the adsorption mass by using Sauerbrey equation [5]. Then, the ΔH can be extracted by combining the obtained adsorption isotherms and Clausius-Clapeyron equation. As

shown in Fig. 6, the ΔH between La/AlPO-5 and NH₃ is -27.59 kJ/mol. Based on classical adsorption theories, the selectivity of reversible physical adsorption is slightly weaker than other adsorption modes when the value of ΔH is in the range of -40 to 0 kJ/mol. Strong chemical reaction would not possess reversibility when the value of ΔH is less than -80 kJ/mol. Taking into account the selectivity and reversibility, weak chemical adsorption is desired for gas sensor when the ΔH value is in the range of -80 to -40 kJ/mol [37]. Obviously, the calculated ΔH values between La/AlPO-5 and NH₃ is belong to physical adsorption.

The effect of humidity cannot be ignored for sensing material based on mass transducer at room temperature. It is obvious that NH₃ can absorb H₂O molecules and form metastable NH₃• α H₂O. Therefore, we explored the humidity-enhanced NH₃ sensing effect of La/AlPO-5 based on the previous research [38]. As shown in Fig. 7a, we listed the response of different concentrations (60 ppb and 180 ppb) of NH₃ under different relative humidity conditions (0% RH and 50% RH). Then, the crystal-water number of NH₃• α H₂O can be worked out by the following equation.

$$\frac{m(\text{NH}_3) + (x - 1)m(\text{H}_2\text{O})}{m((\text{NH}_3))} = \frac{17 + 18(\alpha - 1)}{17} = 2.12 \quad (1)$$

Where α is the crystal-water number. We can calculate the hydrated NH₃ in 50% RH wet air is NH₃•2.05H₂O. Besides, the hydrated NH₃ in

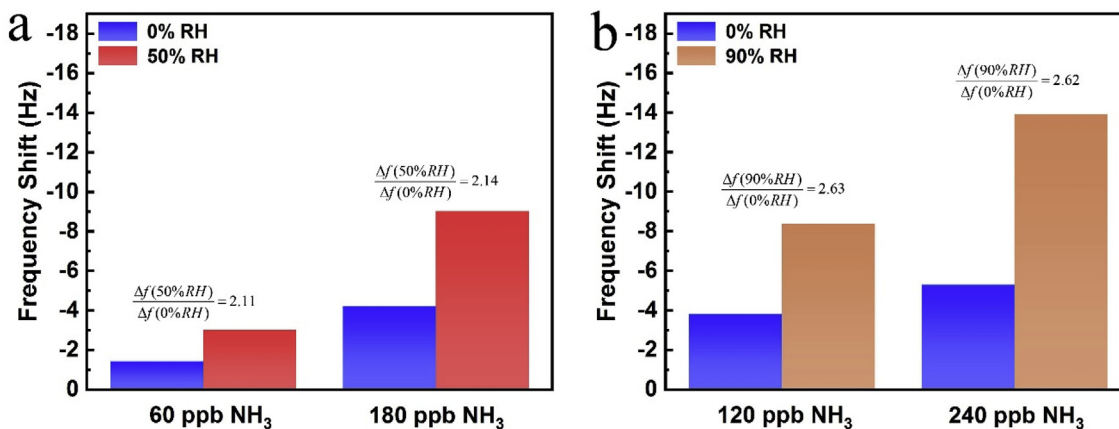


Fig. 7. Comparison of the La/AlPO-5 sensing data obtained under different relative humidity conditions.

90% RH wet air is $\text{NH}_3 \cdot 2.54\text{H}_2\text{O}$, which can be calculated from the data of Fig. 7b. It is obvious that the presence of water molecules can increase the response of La/AlPO-5 to NH_3 because of the formation of hydrating $\text{NH}_3 \cdot \alpha\text{H}_2\text{O}$. But we can measure the molecular formula of hydrated NH_3 under different humidity, and use post-processing, such as error compensation method, to ensure the practicality of the sensing material in the future.

4. Conclusion

In this work, we report a new solid sensing material, La doped AlPO-5, for NH_3 sensing system based on QCM, which works at room temperature with detection limits down to ppb level. Due to the doping of La, the sensing performance of AlPO-5 had been greatly improved. The thermodynamic extraction experiment indicated that the NH_3 sensing performance of La doped AlPO-5 is attributed to physical adsorption, which is in accordance with its fast recovery ability. Besides, environmental humidity can slightly increase the response because of the hydrating $\text{NH}_3 \cdot \alpha\text{H}_2\text{O}$, and further correction is required. The proposed new type of sensing material is expected to be used in practical industries where NH_3 must be used.

Acknowledgments

This work is supported by Young science and technology talents upgrading scheme (Project Number 18SG-15).

References

- P. Dhivya, A.K. Prasad, M. Sridharan, Magnetron sputtered nanostructured cadmium oxide films for ammonia sensing, *J. Solid State Chem.* 241 (2014) 24–29.
- E. Fazio, M. Hjjiri, R. Dhahri, L.E. Mir, G. Sabatino, F. Barreca, F. Neri, S.G. Leonardi, A. Pistone, G. Neri, Ammonia sensing properties of V-doped ZnO:Ca nanopowders prepared by sol-gel synthesis, *J. Solid State Chem.* 226 (2015) 192–200.
- J.W. Erisman, M.A. Sutton, J. Galloway, Z. Klimont, W. Winiwarter, How a century of ammonia synthesis changed the world, *Nat. Geosci.* 1 (2008) 636–639.
- Q. Wei, P. Song, Z. Li, Z. Yang, Q. Wang, Enhanced triethylamine sensing performance of MoO₃ nanobelts by RuO₂ nanoparticles decoration, *Vacuum* 162 (2019) 85–91.
- D. Yan, P. Xu, Q. Xiang, H. Mou, J. Xu, W. Wen, X. Li, Y. Zhang, Polydopamine nanotubes: bio-inspired synthesis, formaldehyde sensing properties and thermodynamic investigation, *J. Mater. Chem.* 4 (2016) 3487–3493.
- L. Wang, Y. Zhu, Q. Xiang, Z. Cheng, Y. Chen, J. Xu, One novel humidity-resistance formaldehyde molecular probe based hydrophobic diphenyl sulfone urea dry-gel: synthesis, sensing performance and mechanism, *Sensor. Actuator. B Chem.* 251 (2017) 590–600.
- F. Temel, M. Tabakci, Calix [4] arene coated QCM sensors for detection of VOC emissions: methylene chloride sensing studies, *Talanta* 153 (2016) 221–227.
- X. Cha, F. Yu, Y. Fan, J. Chen, L. Wang, Q. Xiang, Z. Duan, J. Xu, Superhydrophilic ZnO nanoneedle array: controllable in situ growth on QCM transducer and enhanced humidity sensing properties and mechanism, *Sensor. Actuator. B Chem.* 263 (2018) 436–444.
- V.A. Minha, L.A. Tuan, T.Q. Huy, V.N. Hung, N.V. Quy, Enhanced NH_3 gas sensing properties of a QCM sensor by increasing the length of vertically orientated ZnO nanorods, *Appl. Surf. Sci.* 265 (2013) 458–464.
- X. Li, X. Chen, Y. Yao, N. Li, X. Chen, High-stability quartz crystal microbalance ammonia sensor utilizing graphene oxide isolation layer, *Sensor. Actuator. B Chem.* 196 (2014) 183–188.
- Y. Jia, H. Yu, Y. Zhang, L. Chen, F. Dong, Phenylacetic acid-modified nanofibrous polystyrene membranes for use as highly sensitive ammonia sensors, *Sensor. Actuator. B Chem.* 212 (2015) 273–277.
- Z. Wu, X. Chen, S. Zhu, Z. Zhou, Y. Yao, W. Quan, B. Liu, Enhanced sensitivity of ammonia sensor using graphene/polyaniline nanocomposite, *Sensor. Actuator. B Chem.* 178 (2013) 485–493.
- M. Kikuchi, K. Omori, S. Shiratori, Quartz Crystal Microbalance (QCM) sensor for ammonia gas using clay/polyelectrolyte layer-by-layer self-assembly film, in: *Sensors, 2004. Proceedings of IEEE, IEEE, 2004.*
- X. Wang, J. Zhang, Z. Zhu, J. Zhu, Effect of Pd²⁺ doping on ZnO nanotetrapods ammonia sensor, *Colloid surface. A* 276 (2006) 59–64.
- H. Nanto, Y. Hamaguchi, Y. Yokoi, S. Kurosawa, T. Oyabu, E. Kusano, A. Kinbara, A smart ammonia gas sensor using QCM with plasma-polymerized membrane, *Sensor. Mater.* 13 (2001) 69–76.
- Y. Jia, H. Yu, Y. Zhang, F. Dong, Z. Li, Cellulose acetate nanofibers coated layer-by-layer with polyethylenimine and graphene oxide on a quartz crystal microbalance for use as a highly sensitive ammonia sensor, *Colloid. Surf. B* 148 (2016) 263–269.
- Y. Jia, L. Chen, H. Yu, Y. Zhang, F. Dong, Graphene oxide/polystyrene composite nanofibers on quartz crystal microbalance electrode for the ammonia detection, *RSC Adv.* 5 (2015) 40620–40627.
- S.L. Schiavo, P. Cardiano, N. Donato, M. Latino, G. Neri, A dirhodium (II,II) complex as a highly selective molecular material for ammonia detection: QCM studies, *J. Mater. Chem.* 21 (2011) 18034–18041.
- Y. Jia, C. Yan, H. Yu, L. Chen, F. Dong, One-step fabrication of ammonia sensor by electrospinning PS-b-PMA nanofibers on quartz crystal microbalance, *Sensor. Actuator. B Chem.* 203 (2014) 459–464.
- P. Sun, Y. Jiang, G. Xie, X. Du, X. Li, J. Hu, Layer-by-layer assembly carbon nanotubes thin film based gas sensors for ammonia detection, *Sci. China Inf. Sci.* 54 (2011) 2680–2686.
- Y. Ogimoto, R. Selyanchyna, N. Takahara, S. Wakamatsu, S.W. Lee, Detection of ammonia in human breath using quartz crystal microbalance sensors with functionalized mesoporous SiO₂ nanoparticle films, *Sensor. Actuator. B Chem.* 215 (2015) 428–436.
- J.H. Park, J.H. Ko, S. Hong, Y.J. Shin, N. Park, S. Kang, S.M. Lee, H.J. Kim, S.U. Son, Hollow and microporous Zn–Porphyrin networks: outer shape dependent ammonia sensing by quartz crystal microbalance, *Chem. Mater.* 27 (2015) 5845–5848.
- Y. Zhu, Z. Cheng, Q. Xiang, Y. Zhu, J. Xu, Rational design and synthesis of aldehyde-functionalized mesoporous SBA-15 for high-performance ammonia sensor, *Sensor. Actuator. B Chem.* 256 (2018) 888–895.
- C.M. Chen, J.M. Jehng, Effect of synthesis pH and H₂O molar ratio on the structure and morphology of aluminum phosphate (AlPO-5) molecular sieves, *Catal. Lett.* 85 (2003) 73–80.
- R. Zhao, Y. Wang, Y. Guo, Y. Guo, X. Liu, Z. Zhang, Y. Wang, W. Zhan, G. Lu, A novel Ce/AlPO-5 catalyst for solvent-free liquid phase oxidation of cyclohexane by oxygen, *Green Chem.* 8 (2006) 459–466.
- J. Wang, J. Song, C. Yin, Y. Ji, Y. Zou, F. Xiao, Tetramethylguanidine-templated synthesis of aluminophosphate-based microporous crystals with AFI-type structure, *Microporous Mesoporous Mater.* 117 (2009) 561–569.
- J. Martens, P. Jacobs, Crystalline microporous phosphates—A family of versatile catalysts and adsorbents, *Elservier science B* 85 (1994) 653–685.
- P.J. Grobet, W.J. Mortier, E.F. Vansant, G.S. Eklhoff, Innovation in zeolite materials science, *Stud. Surf. Sci. Catal.* 13 (1988).
- Y. Murakami, A. Lijima, J.W. Ward, New developments in zeolite science and technology, *Stud. Surf. Sci. Catal.* 28 (1986).

- [30] J. Kornatowski, Adsorption isotherms of water as a tool for characterization of metal substituted aluminophosphate molecular sieves, *CR Chim* 8 (2005) 561–568.
- [31] K. Tsutsumi, K. Mizoe, K. Chubachi, Adsorption characteristics and surface free energy of AlPO₄-5, *Colloid Polym. Sci.* 277 (1999) 83–88.
- [32] S. Prasad, R. Vetrivel, Interaction of water molecules with the VPI-5 lattice, *J. Phys. Chem.* 98 (1994) 1579–1583.
- [33] P. Xu, H. Yu, S. Guo, X. Li, Microgravimetric thermodynamic modeling for optimization of chemical sensing nanomaterials, *Anal. Chem.* 86 (2014) 4178–4187.
- [34] S. Guo, P. Xu, H. Yu, Z. Cheng, X. Li, Synergistic improvement of gas sensing performance by micro-gravimetrically extracted kinetic/thermodynamic parameters, *Anal. Chim. Acta* 863 (2015) 49–58.
- [35] J. Zong, Y. Zhang, Y. Zhu, Y. Zhao, W. Zhang, Y. Zhu, Rapid and highly selective detection of formaldehyde in food using quartz crystal microbalance sensors based on biomimetic poly-dopamine functionalized hollow mesoporous silica spheres, *Sensor. Actuator. B Chem.* 271 (2018) 311–320.
- [36] L. Wang, Z. Wang, Q. Xiang, Y. Chen, Z. Duan, J. Xu, High performance formaldehyde detection based on a novel copper (II) complex functionalized QCM gas sensor, *Sensor. Actuator. B Chem.* 248 (2017) 820–828.
- [37] P. Atkins, J.D. Paula, *Atkins' Physical Chemistry*, seventh ed., Oxford University Press, Oxford, 2007, pp. 988–989.
- [38] M. Liu, S. Guo, P. Xu, H. Yu, T. Xu, S. Zhang, X. Li, Revealing humidity-enhanced NH₃ sensing effect by using resonant microcantilever, *Sensor. Actuator. B Chem.* 257 (2018) 488–495.